

## Preparation and optimization of heterojunction donor(DLC) – acceptor(Si) as a solar cell by DFT and PLD

M. H. Kadhim, A. S. Hasan\*, M. A. Akraa, A. Y. Layla  
*Department of Polymer and Petrochemical Industries, College of Materials Engineering, University of Babylon, Babil, Iraq*

Hybrid bilayer heterojunction (DLC) thin-film P-type as an active donor layer and (Si) thin-film n-type as an acceptor with (Electron Transport Layer), were fabricated using Q-switching Nd-YAG Pulsed Laser Deposition (PLD) method under vacuum condition  $10^{-3}$  torr on two electrodes for (AL) Aluminum material is used to construct the hybrid bilayer heterojunction photovoltaic solar cell (PVSC). The electrical properties of hybrid heterojunction Al / DLC / Si / AL thin film were studied. The result showed the voltage of open circuit ( $V_m=0.145V$ ), a short circuit ( $J_m=9.3mA/cm^2$ ), and the fill factor (FF) of (0.4709), with Xenon lamp with an intensity ( $235mw/cm^2$ ), the conversion efficiency ( $\eta=3.54\%$ ) at thickness(75nm). While the theoretical calculations and optimization of the HETEROJUNCTION confirmed the possibility of using it as a successful solar cell, the calculation of the small energy gap and thus the high electrical conductivity, and the determination of the type of charge carriers(p), as well as some electronic properties such as electrostatic potential surfaces and 3-D electron density, hardness, softness and electrophilicity, were clarified.

(Received February 1, 2021; Accepted May 18, 2021)

*Keywords:* Heterojunction, Density functional theory(DFT), Pulsed laser deposition (PLD), Electrical properties

### 1. Introduction

The semiconductors of organic and Inorganic could be categorized into two classes of semiconductors. In the electronic sector, hypothetical inorganic semiconductors such as germanium and silicon are commonly utilized; the semiconductors of organic are also anticipated to be utilized eventually. The highly occupied and lowest unoccupied molecules orbitals (LUMO and HOMO), respectively on the semiconductors of organic is the bands of conduction and the bands of valence. The electrons will move from molecular to molecular (Hopping Mechanism) in the case of semiconductors of organic, while in the case of semiconductors of inorganic in the conduction and valence band move through the material as if they are free. When compared to the semiconductor of inorganic, the hopping transport mechanism provides organic semiconductor rather low mobility. For tiny molecular organic semiconductors, mobility of the hole is obtained up to  $\sim 1.5 \times 10^{-3} m^2 / v.s$  [1, 2], whereas silicone will have the movement of up to approximately  $0.045 m^2.(v.s)^{-1}$  [3]. However, electron movement reaches  $\sim 1 \times 10^{-5} m^2 / v.s$  for some tiny molecular materials. [4,5].

While silicon does have a significantly greater electron movement of  $0.1 m^2.(v.s)^{-1}$ . Low mobility is a significant drawback for the semiconductors of organic comparison with the semiconductors of inorganic [6]. Carbon is a unique element in various types and forms; graphite, diamond, nanotubes, and fullerene. It is formed in the diversity of long, medium, and short-range configurations. Graphite ( $sp^2$ ) is of threefold tetrahedral bonding, while diamond ( $sp^3$ ) is a fourfold tetrahedral bonding[1ab]. Carbon also appears as Diamond-like carbon (DLC), a combination of  $sp^3$  and  $sp^2$  bonding, in another type. The DLC film is very smooth, with an amorphous composition. On multiple substrates, it may be dispersed. Amorphous carbon (a-C) or hydrogenated amorphous carbon (a-C: H) with a substantial fraction of  $sp^3$  bonds is known as diamond like carbon(DLC). A-C: H has another three-content limited (C-C)  $sp$ . Tetrahedral

---

\* Corresponding author: mat.ali.salah@uobabylon.edu.iq

amorphous carbon (ta-C) is labeled DLC with the maximum sp<sup>3</sup> material, and its hydrogenated counterpart is (ta-C: H) [ 7]. is the most used organic compounds as an effective layer in photovoltaic solar cells(PSCs) owing to its multiple maximum absorptions in the visible part of the solar spectrum (less than 700 nm)[ 8,9]. Silicon(Si) was the most frequently used as electron transport layer (ETL) products for inverted solar cells owing to the elevated optical transparency in the visible and near-infrared area, as well as the elevated mobility of carriers. [10].

In this study we used, the (DLC) p-type organic semiconductor is served as an electron donor while the (Si) n-type semiconductor is served as an electron acceptor to prepared hybrid Al/DLC/ Si/AL thin films solar cell. Compared to the acceptor, donor materials have greater LUMO and HOMO. But the donor is the material transporting the hole and ideally makes ohmic contact with the anode while electrons are transported by the acceptor materials and the cathode contact [11,12]. The voltage of open-circuit ( $V_{oc}$ ) of organic photovoltaic machines is identified by the variance between the energy level of donor HOMO and the acceptor LUMO energy level ( $V_{oc} = E_{HOMO}^D - E_{LUMO}^A$ ) [13,14]. Thus, to minimize donor and acceptor energy loss, HOMO and LUMO concentrations should be carefully tuned.

## 2. Experimental measurements

### 2.1. Measurements of Atomic Force Microscope

SPM-AA3000 contact mode spectrometer, Angstrom Advanced Inc., an American company, conducted surface morphological measurements for DLC thin films with different thicknesses. Roughness was obtained computerize, grain size, and 3D images for all studied samples were getting.

### 2.2. Hall effect measurements for DLC thin films

The Hall Effect Measurements are performed using a Hall Effect System (HIMS-3000) provided by the Ecopa Company to estimate the Hall Effect Coefficient (RH), the type of charge carriers, and estimate their mobility and concentration of charge carriers for DLC thin films. The Hall coefficient and Hall mobility are obtained.

### 2.3. Preparation of solar cell devices

Bilayer hybrid organic-inorganic semiconductor photovoltaic solar cell consisting of Diamond-like Carbon (DLC) as electrons donor (p-kind) and acceptor (n-kind) for Silicon (Si) was prepared. Also, the two electrodes, Aluminum (AL) as a Cathode and an Anode, were deposited to contain the bilayer photovoltaic solar cells' devices As shown in the Fig. 1.

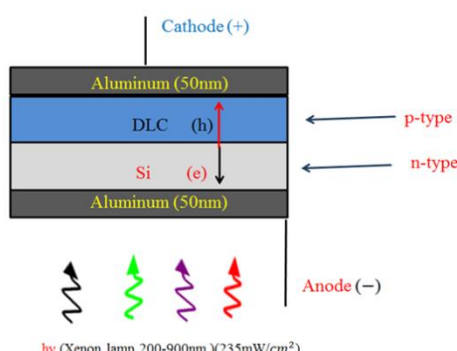


Fig. 1. A schematic view of the DLC/Si heterojunction solar cell bilayer.

### 2.4. Computational details

Because of the technology applications of the organic materials, The present study deals with the computational design of heterojunction and its application in molecular electronics as a solar cell.

The GaussView 5.0.8 program [15] has been utilized to sketch the original configuration of the heterojunction and include the database for the input file. The measurements were carried out utilizing the Gaussian 09 software kit [16]. In order to analyze the structural characteristics of heterojunction donor (DLC)-acceptor (Si) molecular systems and assess their energies, B3LYP/6-31G (d, p) density functional theory (DFT) was used. Under the orbital-vertical principle, the electronic characteristics of such structures were determined based on Koopman's theorem. [15].

The findings indicate that the functions utilized in the definition of the molecular systems investigated have been shown to be accurate in the measurement of geometrical features and are appropriate for the configuration of geometry and the calculation of (LUMO) and (HOMO) energies for organic molecules

## 4. Results and discussions

### 4.1. Atomic Force Microscope

The thin film prepared at 800mJ/cm<sup>2</sup>/6Hz/800Pulse that includes the highest percentage of sp<sup>2</sup> bonds (graphite-like), and the thin film that includes the high percentage of sp<sup>3</sup> bonds (diamond-like) prepared at 300mJ and 2Hz /200pulse, where the films chosen for the AFM Analysis. The surface morphology and granularity DLC films distribution that prepared by the PLD with various laser energy have been studied by AFM, as shown in Fig. 2. It can be observed that the DLC films are regular, homogeneous, smooth structures and composed of spherical and non-spherical small and compact particles of different sizes influenced by the laser energy.

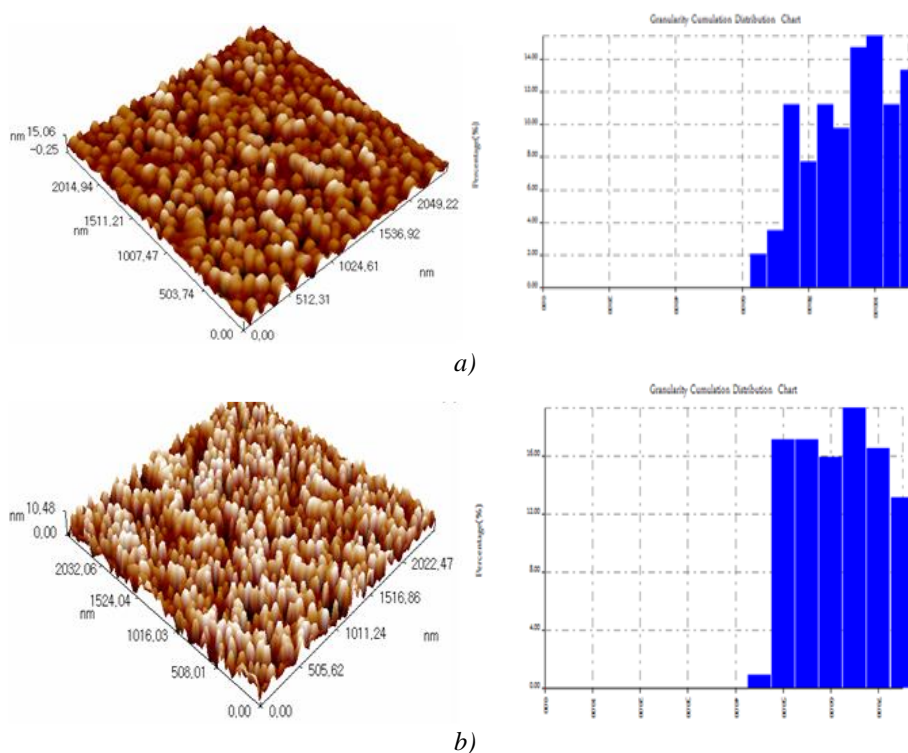


Fig. 2. 3D AFM images of DLC films and particle size distribution (a) 300mJ and 2Hz /200pulse and (b) 800mJ and 6Hz/800pulse.

The average roughness increases with increasing the laser energy[17]. The 300mJ sample has minimum surface roughness magnitudes of root mean square and average particle size. Increasing the laser energy, the average particle size and root mean square of surface roughness increase to reach the maximum values of sample (b), as illustrated in Table (1). The averages of

particle size, roughness, and root mean square of DLC films determined from AFM analysis are indicated to be approximately 59.35nm, 2.54 nm, and 3nm, respectively, for sample (a). These values increase with increasing laser energy to be 89.72 nm, 2.59 nm, and 3.11nm, respectively, for films prepared at laser energy 800mJ, as shown in Table (1). The granularity distribution confirms that particles' sizes are unequal and depend on the mechanism of DLC growth. In greater energies, the atoms have elevated energy to move across the surface and accumulate with the other clusters, causing greater RMS values.

*Table 1. The averages of particle size, roughness, and root mean square for DLC thin films produced as a laser energy function.*

Laser energy	Average particle size (nm)	Average roughness (nm)	root mean square (nm)
300mJ and 2Hz/200pulse	59.35	2.54	3
800mJ and 6Hz/800pulse	89.72	2.59	3.11

The high energies lead to increased substrate temperature increasing roughness due to the diffusional cluster created at the surface. The average kinetic energy of carbon atoms increases due to the increase in temperature affected by the films' nature and the shape. It could be concluded that DLC thin films deposited at 300mJ have more compact, uniform, and smoother, where the nucleus is spherical than DLC films deposited at 800mJ. These properties include the Hall effect, which gives information about the charge carriers' type, concentration, and mobility. The thin film that includes the highest percentage of sp<sup>2</sup> bonds (graphite-like) and the thin film that includes the high percentage of sp<sup>3</sup> bonds (diamond-like) prepared at 800mJ and 6Hz/800pulse and 300mJ and 2Hz/200pulse, respectively, were chosen for this study has a significant function in the films' structure and surface roughness where the increase of surface's roughness and morphology might be recognized to the sp<sup>2</sup> clusters growth, sp<sup>2</sup> clusters ordering [18].

#### 4.2. DLC films electrical characteristics

The measurements of hall demonstrated that all the deposited DLC films were p-type[19]. DLC thin films have a bulk concentration in the range of ( $4.3 \times 10^{12} - 4.7 \times 10^{12} \text{ cm}^{-3}$ ) for laser energy at (300 and 800)mJ, respectively. From Table 2, the increase of the bulk concentration and electrical conductivity with increasing laser energy can be noticed. And that could be attributed to the fact that the 300mJ sample contains more diamond-like sp<sup>3</sup> hybridization types [20]. The sample 800mJ has the maximum values of bulk concentration and low sp<sup>3</sup> carbon atoms content. The electrical resistivity of DLC thin film decreases gradually with the increase of laser energy. The thin films of DLC resistivity is majorly based on sp<sup>2</sup> amount. A greater sp<sup>2</sup> cluster causes a reduction in resistivity [21]. With the lowest laser energy (300mJ), the resistivity value was ( $3.8 \times 10^6 \Omega \cdot \text{cm}$ ), and it decreased to about ( $5.99 \times 10^3 \Omega \cdot \text{cm}$ ) at 800 mJ.

*Table 2. Electrical parameters of deposited DLC thin films by PLD.*

Laser energy m	$\sigma$ ( $\Omega \cdot \text{cm}$ ) <sup>-1</sup>	RH ( $\text{cm}^2/\text{c}$ )	n ( $\text{cm}^{-3}$ ) $\times 10^{12}$	type	$\mu\text{H}$ ( $\text{cm}^2/\text{V} \cdot \text{s}$ )
300 mJ	$2.59 \times 10^{-7}$	$1.44 \times 10^6$	4.3	p	-
800 mJ	$1.66 \times 10^{-4}$	$1.33 \times 10^6$	4.7	p	221

The measurement of hall demonstrates that films of DLC have hole mobility in the ranges of (0–221  $\text{cm}^2/\text{V}\cdot\text{s}$ ) and bulk concentration in the range of  $(4.3\text{--}4.7)\times 10^{12} \text{ cm}^{-3}$  for the sample prepared at laser energy (300 and 800)mJ, respectively, as illustrated in Table (2). The mobility of film increases with increasing laser energy, as demonstrated that the films of DLC contain high  $\text{sp}^2$  structural bonds [22], The thin film that includes the high percentage of  $\text{sp}^3$  bonds (diamond-like), prepared at 300mJ and 2Hz/200pulse, was chosen for the next study. Hall measurements showed that all the deposited DLC films were p-type.

#### 4.3. Current-voltage characteristics results for DLC/Si hybrid bilayer heterojunction

The thin film that includes the high percentage of  $\text{sp}^3$  bonds (diamond-like) was prepared at 300mJ, and 2Hz / 200pulse was chosen from the optimum conditions. The calculation at the usual angle of the incident light of the reflected light from the polished silicon surface indicates a reduction in strength of the reflected light during DLC film deposition. For the following factors, the 300mJ and 2Hz /200pulse samples were chosen as an anti-reflection coating: first, low coefficient of absorption, second, optical energy band gap of approximately 2.38eV, third, low reflection, and lastly, the index of refractive of  $n=1.5$  at 400nm and  $n=1.28$  at 600nm.  $(1 \times 1) \text{ cm}^2$  with Xenon lamp with a strength ( $235\text{mw}/ \text{cm}^2$ ) has been sliced with Silicon solar cell without antireflection coating. DLC thin films produced at (300mJ and 2Hz/200pulse) have been coated with various thicknesses ( $d=35, 55, 75, 100,$  and  $130\text{nm}$ )[23] to choose the optimal film thickness. The I-V properties of these cells as a feature of the thickness of the DLC film are seen in Fig. 3. After applying the antireflection, an improvement has been observed in the solar cell's short circuit current ( $J_{sc}$ ) [22,24].

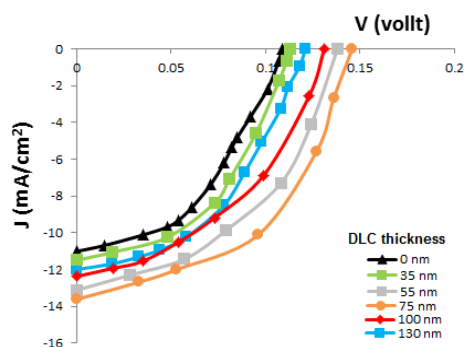


Fig. 3. I-V Characteristic under illumination as a DLC thin thickness film function.

The maximum value of  $J_{sc}$  at  $d=75\text{nm}$ , increasing or decreasing the DLC thickness has decreased the  $J_{sc}$ . Table (3) shows the fill factor (FF) and the conversion efficiency ( $\eta$ ) values for all thicknesses.

Table 3. Values of  $V_m$ ,  $J_m$ , FF, and  $\eta$  for DLC/Si heterojunction.

Thickness (nm)	$J_m(\text{mA}/\text{cm}^2)$	$V_m$	FF	$\eta$ %
0	7	0.075	0.437	2
35	8	0.076	0.467	2.31
55	8.8	0.097	0.471	3.25
75	9.3	0.145	0.4709	3.54
100	8.4	0.082	0.425	2.62
130	8.3	0.08	0.457	2.53

#### 4.4. DFT investigations

The configuration of the HETEROJUNCTION molecular system was conducted at the level of B3LYP/6-31 G (d, p) also with the analysis of population and for the donor and acceptor for comparison study of the configurations of the level of energy of these the system and elements.

The B3LYP/6-31G (d, P) configured structure is seen in Fig. 4. From this figure, could be shown that DLC is a donor and Si is an acceptor.

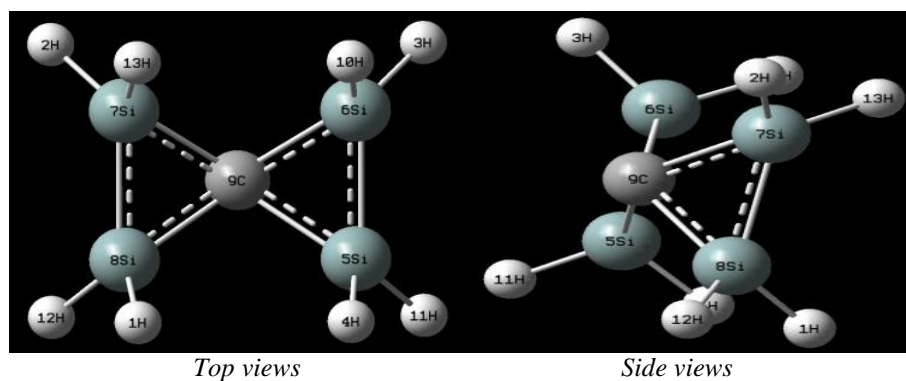


Fig. 4. The optimized geometric structures of heterojunction donor(DLC) – acceptor (Si) as a solar cell.  
Grey: carbon, white: hydrogen, silver: silicon.

The configured atoms coordinate in heterojunction donor is (DLC) and acceptor is (Si) are seen in Table 4.

Table 4. Values of  $V_m$ ,  $J_m$ ,  $FF$ , and  $\eta$  for DLC/Si heterojunction.

Symbol	Bond	Angle	Dihedral	X (Å <sup>0</sup> )	Y (Å <sup>0</sup> )	Z (Å <sup>0</sup> )
H <sub>1</sub>	---	---	---	0	0	0
H <sub>2</sub>	4.343275	---	---	0	0	4.343275
H <sub>3</sub>	4.716148	76.55194	---	4.586836	0	3.24647
H <sub>4</sub>	4.343275	76.55194	0	2.622051	0	-0.62699
Si <sub>5</sub>	1.47	30.41403	75.75545	3.032225	0.7213	0.586433
Si <sub>6</sub>	2.071255	121.5779	-21.7809	3.454248	-0.27726	2.351333
Si <sub>7</sub>	2.929433	90	-84.6517	0.605137	-0.27726	3.032613
Si <sub>8</sub>	2.071255	90	0	0.183114	0.7213	1.267713
C <sub>9</sub>	1.939954	122.856	-91.3565	1.901491	0.869102	2.155833
H <sub>10</sub>	1.47	121.5779	0	3.357761	-1.74078	2.449756
H <sub>11</sub>	1.47	101.3956	123.7353	3.814425	1.827623	0.016246
H <sub>12</sub>	1.47	125.7977	-138.527	-0.77241	1.827623	1.113051
H <sub>13</sub>	1.47	85.44541	121.6895	0.735711	-1.74078	3.076741

Table 4 demonstrates the configured geometrical features of heterojunction structures (Angstrom bonds distances, degree bond angles, and degree dihedral angles) determined using the B3LYP/6-31G (d, P) process. It is apparent from Table (4) that the measurement of geometrical features by the existing approach is in strong alignment with the experimental results for DLC (donor). The bond length for these atoms is caused by the disparity in the numbers of atomic for the conjugated atoms. Table 5 states that the fusion of the Si-Si and C-Si bonds derives from the convergence of their numbers of atomic that describes the Si-H bond gap. [16].

The  $E_g$  of the material is the important factor that can influence the electric current of any material. So the small range hole of the material facilitates the transfer of electrons from the level of HOMO to the level of LUMO when the material retains the frequency light. Besides, electrons have an important function in conjugate frames because their ionization is simple (release or capture of electrons), and this corresponds to the increase in energy and thus the increase in electrical conductivity due to the small energy gap. While we observe an increase in the positive charge carriers and the emergence of the P-type, as shown in Table (2) with Hall effect tests, as in Fig. 5 A and B[15,20].

Fig. 5C and 5D show the electrostatic potential (ESP) surfaces and 3-D electron density (TD) of the heterojunction donor(DLC) – acceptor(Si) obtained from DFT-B3LYP. We note that the ESP distribution is stable and balanced compared to the electrical properties results because the charge is pulled at two ends of the film, and the ESP structure is pulled towards the positive charge. Also, knowledge of charge distributions can determine how a molecule interacts with the same [14,21]. At the same time, TD is an illustration of the chance of finding an electron in a specific location around an atom or molecule. As in Fig. 5D, the electron can be found in regions of high electron density. However, due to the principle of indeterminism, it is not possible to determine the exact position of an electron at any point in time. For a system containing one electron, the electron density is proportional to its wave's operating square since increasing in the surface-area of the samples due to the high rate of surface roughness, and this is consistent with the results of AFM assays[17,20].

Also, to evaluate the electronic and electrical properties of the prepared solar cell and compare its results theoretically, it was using DFT:

$$\mu = \left( \frac{\partial E}{\partial N} \right)_{V(\vec{r}), T} \quad (1)$$

$$\eta = \frac{1}{2} \left( \frac{\partial^2 E}{\partial N^2} \right)_{V(\vec{r}), T} \quad (2)$$

$$S = \frac{1}{2\eta} \quad (3)$$

$$\omega = \frac{\mu^2}{2\eta} \quad (4)$$

where  $\mu$ ,  $\eta$ ,  $S$ , and  $\omega$  are the chemical potential, hardness, softness, and electrophilicity separately. Using Koopman's hypothesis, which depends on the contrasts between the HOMO (highest included subatomic orbital) and LUMO (lowest empty subatomic orbital) energies the unbiased particle. Utilizing a limited contrast guess, the international amounts can be given by [21], which is in excellent agreement with the practical results in terms of better solar cell efficiency(3.54) and increased conductivity when increasing the energy at a thickness of 75 nm[15,23], as in Table 5:

Table 5. The calculated energies of BN nanowire film.

$E_{\text{HOMO}}(\text{eV})$	-10.25878
$E_{\text{LUMO}}(\text{eV})$	-4.18712
$E_g(\text{eV})$	6.072
$S(\text{eV})$	0.165
$\mu(\text{eV})$	-7.223
$\eta(\text{eV})$	3.036
$\omega(\text{eV})$	8.593

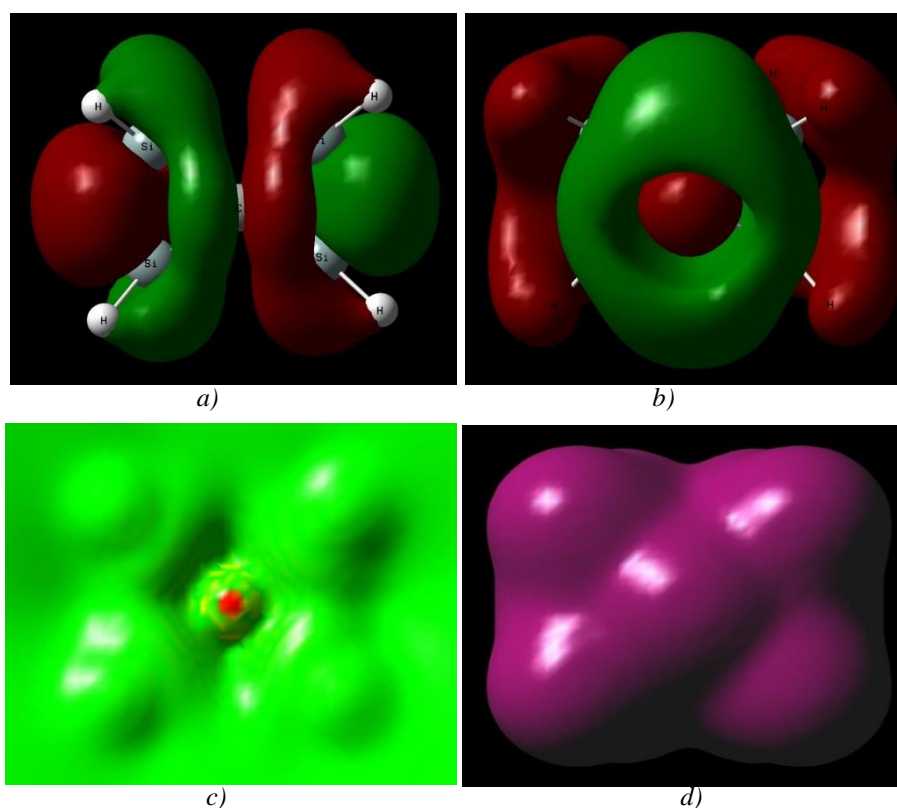


Fig. 5. (a) 3D HOMO distribution and (b) LUMO, (c) The ESP surfaces, and (d) The 3-D TD surfaces of heterojunction donor(DLC) – acceptor(si) as a solar cell.

#### 4. Conclusions

The roughness increases with decreased grain size, which means the largest surface area, the best choice for solar cell making. Hall measurements showed that all the deposited DLC films were p-type. Bilayer heterojunction photovoltaic solar cell device manufacturing gives suitable efficiency, and the efficiency of solar cells has improved after applying DLC thin film as an antireflection coating. The best thickness of DLC film was 75nm. The solar cell's theoretical results also showed the high compatibility between it and the practical results in terms of cell efficiency and increased electrical conductivity due to the proximity of HOMO and LUMO values, and thus the small value of the energy gap.

#### References

- [1] T. D. Anthopoulos, B. Singh, N. Marjanovic, N. S. Sariciftci, A. Montaigne Ramil, H. Sitter, D. M. de Leeuw, *Applied Physics Letters* **89**(21), 213504 (2006).
- [2] D. J. Gundlach, *J Appl Phys* **98**(6), 064502, (2005).
- [3] I. McCulloch, M. Heeney, C. Bailey, K. Genevicius, I. MacDonald, M. Shkunov, D. Sparrowe, S. Tierney, R. Wagner, W. Zhang, M. L. Chabinyc, R. J. Kline, M. D. McGehee, M. F. Toney, *Liquid/crystalline semiconducting polymers with high charge-carrier Mobility*, 2006.
- [4] M. Akraa, A. S. Hasan, M. J. Kadhim, *Baghdad Science Journal* **17**(3), 0795 (2020).
- [5] D. J. Gundlach, *J Appl Phys* **98**(6), 064502 (2005).
- [6] L. J. Koster, *Appl Phys Lett* **88**(9), 093511 (2006).
- [7] H. Zhu, J. Wei, K. Wang, D. Wu, *Solar energy materials and solar cells* **93**, 1461 (2009).

- [8] A. Ferrari, J. Robertson, *Phys. Rev. B* **61**, 20 (2000).
- [9] William H. Brown, Christopher S. Foote, Brent L. Iverson, Eric V. Anslyn, *Organic Chemistry*, Sixth Edition, 2012.
- [10] Ali A. Ati, Alyaa H. Abdalsalam, Ali S. Hasan, *Journal of Materials Science: Materials in Electronics*, 1 (2021).
- [11] J. F. Guillemoles, L. Kronik, D. Cahen, U. Rau, A. Jasenek, H. W. Schock, *J. Phys. Chem. B* **104**, 4849 (2000).
- [12] S. Touaiti, A. Hajri, M. S. Kahwech, B. Jamoussi, *International Journal of Materials Science and Applications* **2**, 179 (2013).
- [13] C. J. Brabec, N. S. Sariciftci, J. C. Hummelen, *Adv Funct Mater* **11**, 15 (2001).
- [14] M. C. Scharber, D. Wuhlbacher, M. Koppe, *Adv Mater* **18**, 789 (2006).
- [15] A. S. Hasan, F. Q. Mohammed, M. M. Takz, *Journal of Mechanical Engineering Research and Developments* **43**, 11 (2020).
- [16] A. S. Hasan, B. Y. Kadem, M. A. Akraa, A. K. Hassan, *Digest Journal of nanomaterials and biostructures* **15**(1), 197 (2020).
- [17] A. Modabber Asl, P. Kameli, M. Ranjbar, H. Salamati, M. Jannesari, *Superlattices and Microstructures*, 1016 (2015).
- [18] S. Kataria, S. Dhara, H. C. Barshilia, S. Dash, A. Tyagi, *J. Appl. Phys.* **112**, 023525 (2012).
- [19] S. Meskinis, R. Gudaitis, V. Kopustinskas, S. Tamulevicius, *Applied Surface Science* **254**, 52525256 (2008).
- [20] Burak Y. Kadem, Mohammed Al-Hashimi, Ali S. Hasan, Raheem G. Kadhim, Yaquab Rahaq, Aseel K. Hassan, *Journal of Materials Science: Materials in Electronics* **29**, 19287 (2018).
- [21] D. Xu-Li, L. Qing-shan, K. Xiang-He, *Chin. Phys. Lett.* **26**, 1 (2009).
- [22] D. Mao, W. Li, X. Wang, X. Liu, *Sur. Coat.Tech.* **137**, 1 (2001).
- [23] W. S. Choi, K. Kim, J. Yi, B. Hong, *Materials Letters* **62**, 577 (2008).
- [24] M. Alalut, J. Appelbaum, D. Scheimanb, N. Croitoru, *Thin Solid Films* **25**, 1 (1995).